Spectrochimica Acta Part A: Molecular and Biomolecular Spectroscopy 290 (2023) 122303

Contents lists available at ScienceDirect

Spectrochimica Acta Part A:
Molecular and Biomolecular Spectroscopy

journal homepage: www.journals.elsevier.com/spectrochimica-acta-part-a-molecular-and-biomolecular-spectroscopy

A journey across dopamine Metabolism: A rotational study of DOPAC

Miguel Sanz-Novo [a], Lucie Kolesniková [b], Aran Insausti [c], José L. Alonso [a], Iker León [a], Elena R. Alonso [a,*]

[a] Grupo de Espectrocopía Molecular (GEM), Edificio Quifima, Laboratorios de Espectroscopía y Bioespectroscopía, Unidad Asociada CSIC, Parque Científico UVa, Universidad de Valladolid, 47011, Valladolid, Spain
[b] Department of Analytical Chemistry, University of Chemistry and Technology, Technická 5, 166 28 Prague 6, Czech Republic
[c] Departamento de Química Física, Facultad de Ciencia y Tecnología, Universidad del País Vasco (UPV/ EHU), 48940 Leioa, Spain

HIGHLIGHTS

- DOPAC (3-dihydroxyphenylacetic acid) is a relevant scaffold in dopamine metabolism.
- DOPAC was transferred in the gas phase and probed by high-resolution rotational spectroscopy.
- Union of laser ablation and rotational spectroscopy provides accurate structural data.
- Three distinct structures of DOPAC have been identified by rotational spectroscopy.

GRAPHICAL ABSTRACT

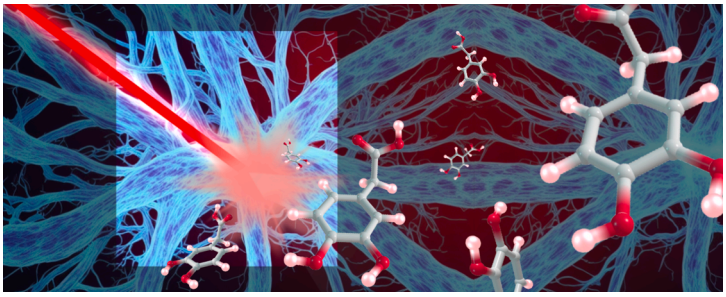

ARTICLE INFO

Keywords:
Neurotransmitters
Conformational panorama
High-resolution spectroscopy
Rotational spectroscopy

ABSTRACT

DOPAC, a relevant scaffold in dopamine metabolism, was probed in the gas phase and interrogated by high-resolution rotational spectroscopy. Herein, three distinct conformers were isolated in a supersonic jet and identified for the first time through an examination of the trend of the rotational constants and the dipole moment selection rules. Additionally, we examined the plausible relaxation pathways of the low-energy conformers of DOPAC, which helped us to claim the indirect detection of two additional conformers, providing conclusive experimental evidence of the flexible nature of this biomolecule. The current investigation sheds some light on the differences between jet-cooled rotational experiments and matrix-isolation infrared spectroscopy.

1. Introduction

Neurotransmitters are molecules involved in the chemical signaling processes in the brain. G-protein–coupled receptors (GPCRs) interact with the neurotransmitters and transmit the information through chemical interactions that commonly occur through the “lock-and-key” interaction model. [1] In the acceptor-receptor interactions of neurotransmitters with GPCRs, it is assumed that the molecules present specific complementary geometric shapes.

GPCRs receptors are a large group of molecules involved in diverse biological functions, and they are one of the major research focuses in pharmacology. [2–3] Concretely, one of the most studied GPCRs is the dopamine receptor, whose primary endogenous ligand is the dopamine (DA) molecule. Dopamine is very common in the vertebrate nervous

* Corresponding author.
E-mail address: elenarita.alonso@uva.es (E.R. Alonso).

https://doi.org/10.1016/j.saa.2022.122303
Received 5 November 2022; Received in revised form 27 December 2022; Accepted 28 December 2022
Available online 31 December 2022

system. This hormone and its receptors affect movement, emotions, and the reward system in the brain. Therefore, it is no surprise that dopamine and its receptors are involved in many diseases, such as Parkinson's and schizophrenia. [4–5] This has led to dopamine and its metabolites being a new target for studying and detecting different diseases. Nowadays, there is growing attention on studying DA metabolic pathways (see Fig. 1) [6–7] to understand dopamine-related biological functions. Precise knowledge of the properties of DA precursors and metabolites becomes essential to discovering and developing new drugs against several degenerative diseases.

In dopamine metabolism, some studies in mice and rats using brain microdialysis samples combined with liquid chromatography have demonstrated that the primary metabolites of dopamine are 3-dihydroxyphenylacetic acid (DOPAC) and homovanillic acid (HVA) (see Fig. 1). [8] HVA does not present very high biological activity and may be considered the last link of dopamine metabolism. However, the DOPAC molecule, one of the most abundant intermediate in dopamine catabolism, is involved in diverse biochemical reactions. For example, in the signaling processes, some studies showed that DOPAC acts as a dopamine agonist in GPCRs and could have an antagonistic effect on GABAρ1 receptor. [9–10] It was also confirmed that the DOPAC molecule interacts with α-synuclein protein, the central molecule involved in synucleinopathy diseases. [11–13] Furthermore, related to the DA metabolism, the patient with Parkinson's and schizophrenia presents alterations in the DOPAC molecule's bio-production through DA's metabolism. [14–15] For this reason, DOPAC is an excellent biomarker to identify the loss of dopaminergic neurons. [16–17] All this indicates that the DOPAC molecule is not a negligible product in dopamine metabolism and is also involved in several biological processes and disorders.

Dopamine has been primarily studied as the principal neurotransmitter molecule, bare and in the enzyme-ligand complexes. [18–20] Besides, advanced techniques using laser vaporization methods have shown its intrinsic structure in isolation conditions, presenting a very rich conformational landscape with seven detected conformers. [21] Moreover, our group has made great efforts to report structural data on the related L-tyrosine [22] and L-DOPA [23], and we plan to extend these investigations to ultimately cover the complete metabolic route of dopamine (see Fig. 1). In this context, little is known about the conformational properties of the DOPAC molecule. Even though DOPAC is expected to present similar conformational flexibility as dopamine, experimentally, only one conformer was detected in both argon and xenon cryogenic matrices. [24] *In-silico,* the authors predicted the possibility of detecting four conformers, so they attributed the non-observation of more conformers to the molecular interconversion to the most stable one. The crystal structure did not bring much information about its conformational landscape because they formed hydrogen-bonded dimers in the crystal lattice, characteristic of the carboxylic acids. [25].

The intrinsic conformational preferences of DOPAC and the possible intramolecular interactions responsible for their stabilizations become fundamental to understanding the biological media's dopamine metabolomics. In this context, we present a comprehensive study of DOPAC using the combination of laser-vaporization, jet-cooled rotational spectroscopy, and high-level density functional theory (DFT) calculations.

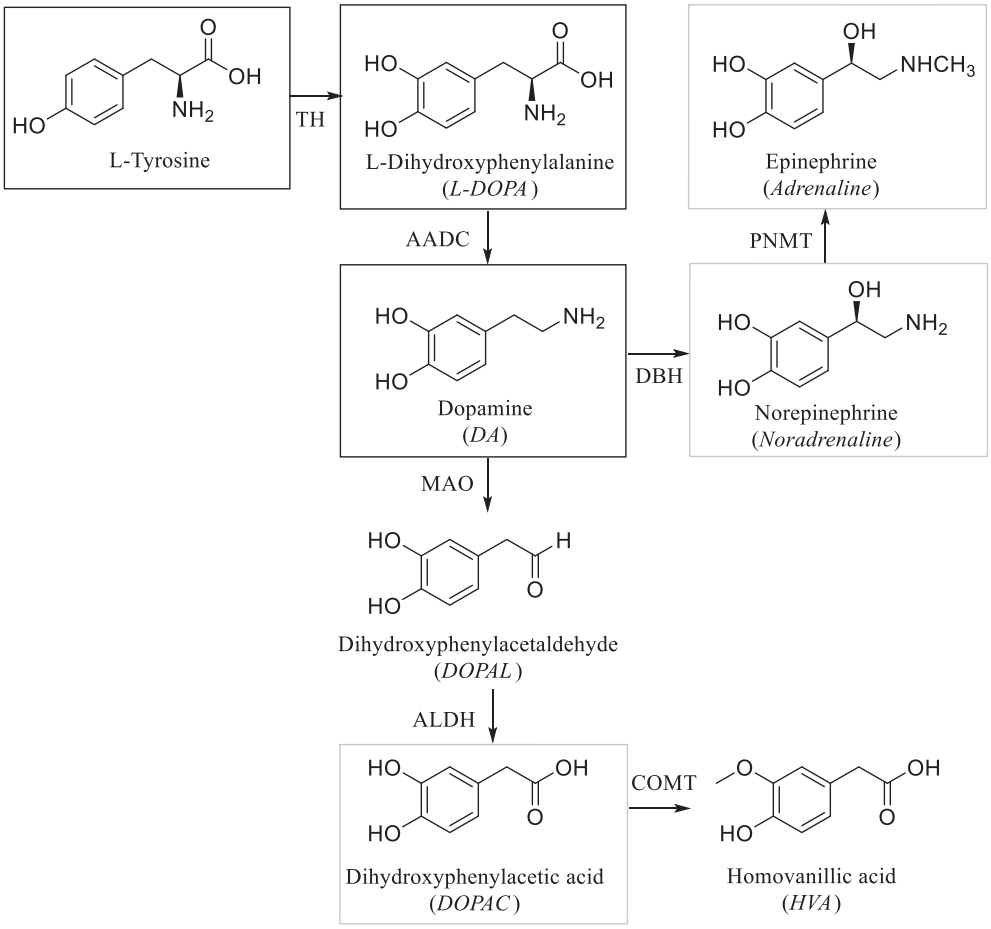

Fig. 1. Schematic classical biosynthesis and degradation pathways of dopamine. [26] We highlight in solid black squares molecules that have already been studied in our laboratory, while in grey squares, we remark molecules currently being investigated, including DOPAC.

2. Methodology

2.1. Theoretical calculations

The unequivocal conformational assignment of the observed rotameric species is generally achieved by directly matching the experimentally determined rotational constants with those predicted theoretically for a set of candidate structures. Although several sets of theoretical calculations are already available in the literature [24] we performed our theoretical computations to estimate other parameters relevant to our experiments, such as the electric dipole moment components, besides rotational constants. Keeping in mind the five possible rotations around single bonds shown in Fig. 2, a systematic conformational search was conducted. In a first step, we employed fast molecular mechanics methods (MMFFs) with the "Large scales Low Mode" and Monte Carlo-based search algorithms in MacroModel (www.schrodinger.com) to locate all possible minima energy structures on the potential energy hypersurface. Subsequently, each molecular structure was further geometrically optimized at the B3LYP-GD3BJ/aug-cc-pVTZ level of the theory (Gaussian 09 package [27]) with Grimme D3 dispersion and Becke-Jonson damping taken into consideration, which is portrayed as the best performing level of theory for dopamine-related molecules (see Appendix A, Theoretical benchmark for additional details). Finally, frequency calculations were performed to identify the stationary points as true minima (all their frequencies are real) and calculate the Gibbs Free Energies. The structures of the five lowest-energy conformers are shown in Fig. 2, and their spectroscopic properties are collected in Table 1. We follow the notation used in a previous study of the structurally similar neurotransmitter dopamine to label these conformers. [28] A combination of three symbols is employed: a capital letter G or A specifies the *gauche* (folded) or *anti* (extended) arrangement of the $-CH_2COOH$ chain, the Roman numerals indicates the energy order (ΔE) for the different conformations related to the position of the *cis* − COOH group with respect to the direction of catechol hydroxyl (–OH) groups, and subscripts *a* and *b* denote the diverse orientations of the catechol − OH groups.

2.2. Experimental methods

A commercial sample of DOPAC (m.p. > 127–130 °C) was finely powdered and blended with a commercial binder. Then the mixture was pressed using a hydraulic press to form approximately 2 cm long cylindrical rods. Small amounts of an adequate binder (methylcellulose, 5 %) are necessary to give enough consistency to the solid rod. Afterward, we employed a Nd:YAG picosecond laser (355 nm, 10 mJ per pulse) to vaporize the sample. We employ a motor controller which allows a DC motor (Oriel Motor Mike 18074) to rotate and translate the rod up and down along the injection system to achieve homogeneous exploitation of the rod. Also, the repetition rate of the experiment is set to 2 Hz to preserve good vacuum conditions in the vacuum chamber and reduce sample consumption. Afterwards, the vaporized products were supersonically expanded into the vacuum chamber of the spectrometer using the pulsed flow of a light inert carrier gas (Ne at a backing pressure of 10 bar), and then probed by microwave spectroscopy. In our laser ablation broadband chirped pulse Fourier transform microwave spectrometer (LA-CP-FTMW), [29] a 24 Gsamples/s arbitrary waveform generator (Tektronix AWG7122B) creates a fast chirp microwave pulse, which is subsequently amplified using a 300 W traveling wave tube amplifier (IFI, GT186-300) to macroscopically polarize the molecules at frequencies from 6.0 to 12.0 GHz. Up to 80.000 individual Free Induction Decays (four FIDs on each valve cycle) were averaged in the time domain and Fourier-transformed to obtain the frequency domain spectrum. We used a Kaiser–Bessel window to improve the baseline resolution. The uncertainty of the line measurements was estimated to be better than 20 kHz. Also, since the sample injection is perpendicular to the microwave field, the transit time of the polarized molecular jet is relatively short and we usually achieve line widths (full-width-half-maximum, FWHM) of approximately 100 kHz.

3. Results and discussion

The broadband CP-FTMW spectrum of laser-ablated DOPAC between 6 and 12 GHz is shown in Fig. 3. A few lines corresponding to photofragmentation products such as vinylacetylene (CH_2CHC_2H) or vinyldiacetylene (CH_2CHC_4H) were quickly spotted and eliminated. The remaining, relatively rich spectrum was then carefully overviewed. According to the values of the rotational constants in Table 1, all conformers will show the characteristic pattern of a near-prolate asymmetric top. Among the dominating features of the spectrum, a characteristic *a*-type *R*-branch progression assigned to $K_a = 1 \leftarrow 1$ transition exemplified in Fig. 3, could be easily recognized and was ascribed to the first rotameric species labeled as rotamer I. In the course of the analysis, weaker lines following practically identical spectral patterns were discovered on the right side of *a*-type *R*-branch transitions

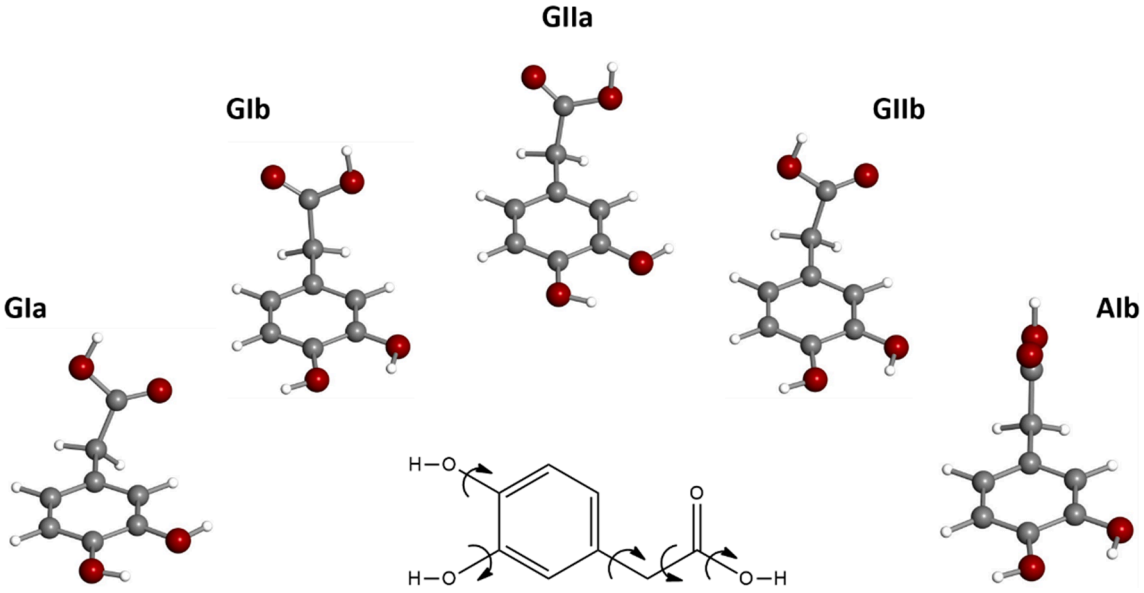

Fig. 2. The five lowest-energy conformers of DOPAC were calculated at the B3LYP-GD3BJ/aug-cc-pVTZ level.

Table 1
Experimental and predicted spectroscopic parameters for the DOPAC conformers.

Experimental				Theory [a]				
Parameter [b]	Rotamer I	Rotamer II	Rotamer III	GIa(II)	GIb(I)	GIIa(III)	GIIb	AIb
A /MHz	1998.53474 (67) [c]	1932.52255 (43)	1979.58731 (59)	**1940.9**	**1998.3**	**1977.7**	**1946.5**	**2236.6**
B /MHz	521.91410 (19)	533.58405 (16)	525.42333 (30)	**533.5**	**522.8**	**526.6**	**530.6**	**480.6**
C /MHz	453.32765 (17)	455.20909 (19)	452.99409 (32)	**455.4**	**453.7**	**454.0**	**456.9**	**438.2**
Δ_J /kHz	0.06255 (80)	0.04321 (86)	0.0397 (17)	…	…	…	…	…
Δ_{JK} /kHz	0.8478 (43)	0.3578 (47)	0.619 (12)	…	…	…	…	…
Δ_K /kHz	1.130 (67)	…	…	…	…	…	…	…
δ_J /kHz	0.01269 (34)	…	…	…	…	…	…	…
δ_K /kHz	−0.586 (48)	…	…	…	…	…	…	…
$\lvert\mu_a\rvert$/D	Observed [d]	Observed	Not observed	**0.7**	**1.9**	**0.2**	**1.8**	**0.5**
$\lvert\mu_b\rvert$/D	Observed	Observed	Observed	**0.4**	**0.9**	**3.2**	**3.6**	**2.1**
$\lvert\mu_c\rvert$/D	Not observed	Observed	Observed	**0.3**	**0.1**	**1.1**	**0.3**	**0.9**
N	75	79	48	…	…	…	…	…
σ_{rms} /kHz	3.5	6.4	8.6	…	…	…	…	…
ΔE / cm^{-1}	…	…	…	**0**	**106**	**128**	**147**	**156**
ΔG / cm^{-1}	…	…	…	**108**	**100**	**168**	**166**	**0**

[a] Calculated at the theory's B3LYP-GD3BJ/aug-cc-pVTZ level with Grimme dispersion. [b] A, B, and C are the rotational constants; Δ_J, Δ_{JK}, Δ_K, δ_J, and δ_K are the quartic centrifugal distortion constants (A-reduction); $|\mu_a|$, $|\mu_b|$ and $|\mu_c|$ are the absolute values of the electric dipole moment components along the inertial axis a, b, c; N represents the number of distinct frequency lines in the fit; σ_{rms} is the root mean square deviation of the fit; ΔE and ΔG represent the relative energy (including ZPE correction) and Gibbs free energy ($T = 298$ K), respectively, to the global minimum. [c] The numbers in parentheses are 1σ uncertainties in the last decimal digit units. [d] Experimental observation of a given type of transition.

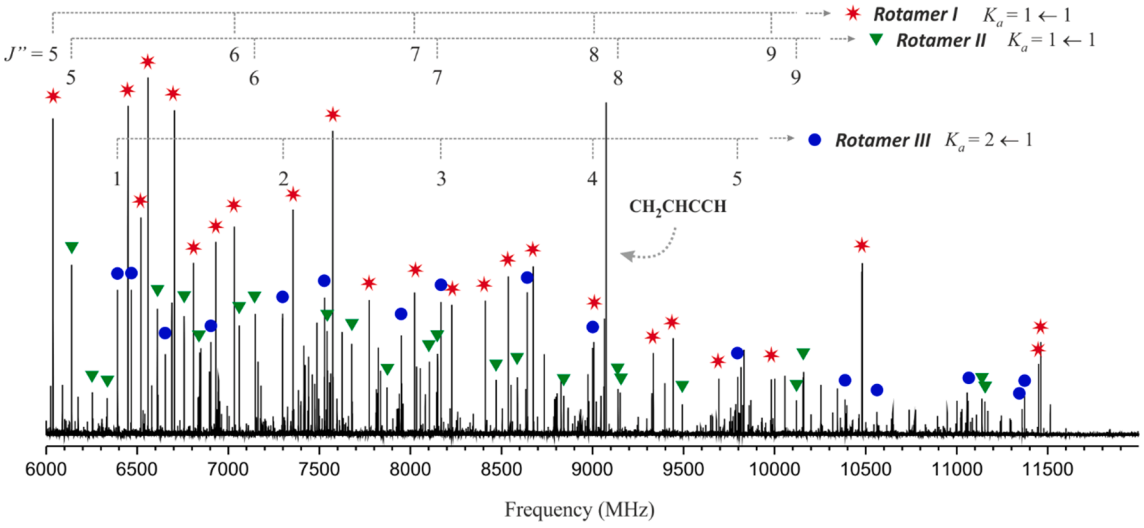

Fig. 3. Broadband rotational spectrum of 3,4-dihydroxyphenylacetic acid measured by LA-CP-FTMW spectroscopy. Corresponding symbols highlight the most prominent lines for each of the detected rotamers. A progression of $K_a = 1 \leftarrow 1$ a-type R-branch transitions is illustrated for rotamers I and II, while $K_a = 2 \leftarrow 1$ b-type R-branch progression is shown for rotamer III. A decomposition line belonging to vinylacetylene is also indicated.

of rotamer I. These satellite lines were attributed to a-type R-branch transitions of rotamer II (see Fig. 3). The possibility that these satellites should be assigned to the vibrationally excited state of rotamer I could be ruled out by the nature of the experiment; this would be significantly depopulated at the low temperature achieved in the supersonic expansion. An iterative procedure of fittings and predictions made it possible to identify b-type R-branch and Q-branch transitions for both rotamers. However, transitions obeying c-type selection rules were observed only for rotamer II. Once the rotational lines of rotamers I and II were removed from the broadband spectrum, new sets of b-type and c-type transitions attributable to rotamer III were found (see $K_a = 2 \leftarrow 1$ progression in Fig. 3). Finally, a-type transitions were predicted but not observed for rotamer III. All rotational transitions collected for these three rotamers were submitted to the analysis employing Watson's asymmetric top semirigid-rotor Hamiltonian in A-reduction and I^r-representation. Obtained spectroscopic constants are collected in the first three columns of Table 1. The measured experimental frequencies are gathered in Tables B1 – B3 of Appendix B.

Rotational constants critically depend on the mass distribution of each rotamer, and their values are usually conclusive in the conformational assignments. However, an inspection of Table 1 shows that the observed rotamers have similar values of the rotational constants as corresponding to conformers with similar mass distributions. These values are only consistent with those predicted for the *gauche* conformers GIa, GIb, GIIa and GIIb, but the differences are not sufficiently significant to discriminate between them unambiguously. In cases like this, one needs to call for another discriminating tool. We can profit from the fact that the values of the dipole moment components drive the rotational selection rules. Hence, the observation or nonobservation of a given type of rotational transition can be, in favorable cases, taken as a definitive tool in the conformational assignments. Rotamer III is the only species for which no a-type transitions were observed. According to Table 1, this observation is only consistent with the predicted nearly zero value of μ_a dipole moment component for conformer GIIa to which rotamer III should be assigned.

Out of the two remaining rotamers (I and II), three candidates still

exit: GIa, GIb, and GIIb. No c-type transitions were found in the records for rotamer I, while the opposite is true for rotamer II, which directly points to rotamer I as conformer GIb. This assignment can be further confirmed by evaluating differences in the values of the rotational constants of GIb conformer using those for the already assigned GIIa as reference. These two conformers differ only in the opposite orientation of the catechol hydroxyl groups (see Fig. 4). This subtle structural change induces a small but specific change in the values of rotational constants. Hence, in going from GIb to GIIa conformer, the predicted changes in rotational constants are $\Delta A = -20.6$ MHz, $\Delta B = 3.7$ MHz, and $\Delta C = -0.3$ MHz, and these nicely match with the observed changes of $\Delta A = -18.95$ MHz, $\Delta B = 3.51$ MHz, and $\Delta C = -0.33$ MHz passing from rotamer I to rotamer III, thus confirming the identification of rotamer I to GIb and rotamer III to GIIa (see Fig. 4).

Rotamer II, which exhibits all dipole moment selection rules, can be ascribed to either GIa or GIIb conformers. The question of which one should be assigned cannot be answered directly. Once again, we invoked the trend of variation in rotational constants in Fig. 4. Conformers GIIa and GIa differ in the orientation of the carboxylic group, producing distinctive shifts in rotational constants that can support the assignment. As shown in Fig. 4, the predicted changes in rotational constants in going from GIIa and GIa are in good agreement with those experimentally derived in going from rotamer III to rotamer II, leading to the conclusion that rotamer II is GIa. Moreover, in this case, the predicted $|\mu_b|$ and $|\mu_c|$ dipole moment components for conformers GIa ($|\mu_b|_{GIa} = 0.4$ D and $|\mu_c|_{GIa} = 0.3$ D) and GIIb ($|\mu_b|_{GIIb} = 3.6$ D and $|\mu_c|_{GIIb} = 0.3$ D) are different. This fact is expected to generate a noticeable difference in relative intensities when comparing the corresponding *b*- and *c*-type transitions of conformers GIa and GIIb, respectively. Consequently, since we observe *b*- and *c*-type lines of comparable intensity for rotamer II it is reasonable to ascribe it to conformer GIa, further corroborating the assignment.

Finally, we pursued the spectrum analysis to search for the other low-energy conformers. A priori, we could expect that both GIIb and AIb conformers should be indeed present in the supersonic expansion since: a) The more extended conformer, AIb, is predicted to be the most abundant species at 298 K (attending to ΔG), b) The abundance of GIIb should be similar to that of GIa, and also its large dipole moment components should ease the conformational search. Note that relative populations at the hypothetical equilibrium of the lowest-energy conformers of DOPAC (at 298 K) have been calculated from the Gibbs energies at the B3LYP/aug-cc-pVTZ level, given in Table 1, to be GIa ≈ 19 %, GIb ≈ 20 %, GIIa ≈ 14 %, GIIb ≈ 14 % and AIb ≈ 32 %. However, no spectral signatures attributable to the GIIb and AIb conformers were found, requiring a deeper analysis. This behavior could be ascribed to plausible conformational interconversion processes, also known as conformational cooling. It is well established that for jet-cooled rotational experiments, conformational relaxation can occur through collisions with the carrier gas if the interconversion barriers are low enough (about ~ 400 cm^{-1} and lower), [29–32] as observed, for instance, for several amino acids and dipeptides. [33–35] Thus, we have examined the corresponding interconversion barriers to test whether the same process is occurring. As shown in Fig. 5, calculated interconversion barriers between conformer AIb and conformer GIb, and between conformer GIIb and AIb are 22 and 190 cm^{-1}, respectively, which helps us rationalize the absence of conformers GIIb and AIb in the supersonic expansion. At this point, we performed relative intensity measurements on different *b*-type transitions of conformers GIa, GIb, and GIIa, since the intensities are proportional to the square of the corresponding dipole moment components. We observed a clear predominance of conformer GIb (about ~ 55 %), which is in great discrepancy with the predicted abundances based on ΔG. This points to a population transfer from either the AIb or GIIb conformers into conformer GIb, which appears enriched in the spectrum, and help us to indirectly corroborate the existence of both AIb and GIIb conformers in the jet.

Additionally, the relaxation process can be confirmed by direct

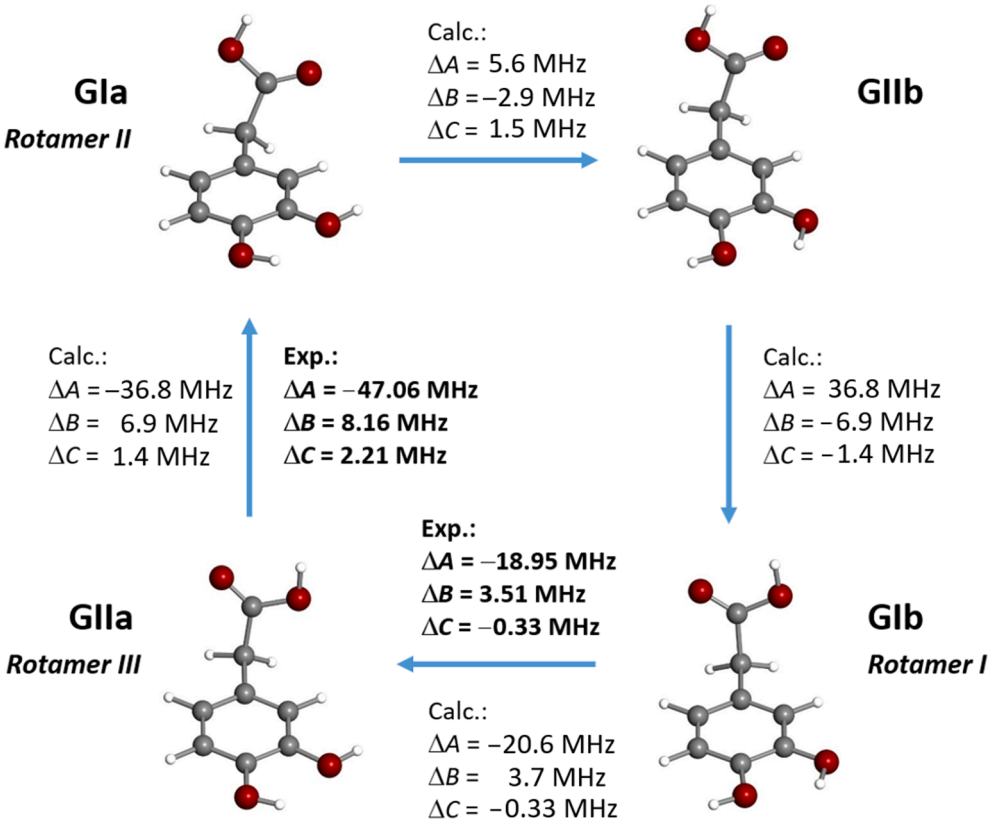

Fig. 4. Experimental and calculated changes in rotational constants induced by the different orientations of the catechol hydroxyl and *cis* carboxylic groups.

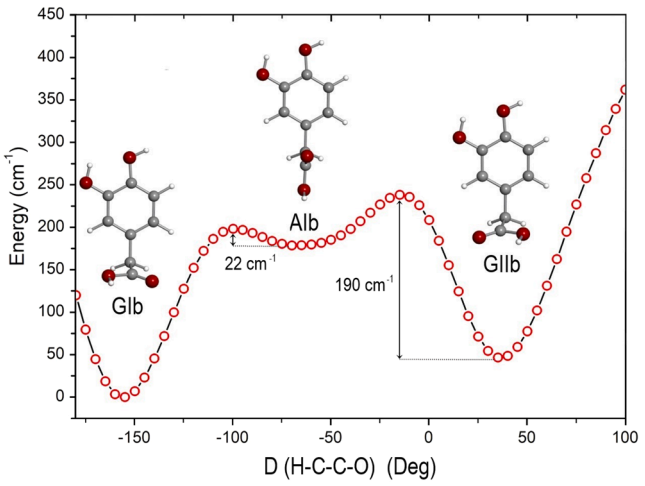

Fig. 5. Calculated relaxed potential energy surface (PES) varying the D (H—C—C—O) dihedral angle (at the B3LYP-GD3BJ/6–311++G(d,p) level). As can be seen, conformer GIIb experiences conformer interconversion into conformer AIb, which further undergoes conformer relaxation into conformer GIb. Therefore, both species are "missing" in the expansion.

comparison with the related L-DOPA. [23] In contrast to DOPAC, the introduction of a polar side chain (NH_2 group) in L-DOPA hampers the interconversion due to the formation of stabilizing OH—N intramolecular hydrogen bonds, which hinders the rotation of the H—C—C—O dihedral angle. Hence, all the low-energy conformers are detected in the supersonic expansion for L-DOPA, while only three conformers, which exhibit a *cis* configuration of the carboxylic group, are conclusively characterized for DOPAC. Nevertheless, current results provide compelling evidence of the whole conformational landscape of DOPAC and complete the previous study by matrix-isolation infrared spectroscopy, [24] where only the most stable GIb conformer survived upon matrix deposition and was subsequently observed. Moreover, our results point out the notorious differences between the characteristic cooling of the supersonic jet, attributed to collisions with the carrier gas, and the conformational cooling corresponding to matrix isolation techniques, [34,35] which exhibit a radically different nature. For the latter, contrary to jet-cooled rotational experiments, barrier heights of about 400 cm^{-1} are not high enough to preclude conformational interconversion processes. [23] Therefore, this conformational relaxation process should be more accused during the deposition process in the matrix as the higher-in-energy conformers appear depopulated in the matrix after deposition. Present results can be used as relevant benchmark information when comparing both spectroscopic environments.

A comparison between the conformational landscapes of DOPAC, L-DOPA, and dopamine brings to light relevant insights. We observe that dopamine-related species exhibit a relatively wide conformational space. The broader panorama is obtained for dopamine, where eighteen conformers are predicted below 600 $cm^{-1,}$ and seven are observed experimentally, all of them exhibiting NH—π stabilizing interactions. A slightly narrower landscape for L-DOPA - seven conformers predicted below 600 cm^{-1} and four conformers detected (plus two tentative observations) -, DOPAC, with only five conformers predicted below 200 cm^{-1} and three observed in the experiment , and tyrosine, the latter exhibiting eight predicted conformers in the same energetic window and only two are observed experimentally. This leads to the following trend for the number of observed conformers (n): dopamine (7) > L-DOPA (6) > DOPAC (3) > tyrosine (2).

As can be seen, tyrosine presents a rather poor conformational space, which is most likely due to severe photofragmentation issues found for aromatic amino acids that usually make challenging the observation of their complete conformational panorama. Nevertheless, the other dopamine-related species exhibit great flexibility. Although, as explained below, in the case of DOPAC the lack of an $–NH_2$ group allows several conformational interconversion processes to occur, which will be directly related to the observation of a somewhat narrower conformational panorama..

4. Conclusions

In the present work, we report a state-of-the-art spectroscopic study of DOPAC, a relevant dopamine metabolite, to shed light on its intrinsic conformational properties. Three distinct structures have been unequivocally identified in the jet, showing a *cis* configuration for the carboxylic group in all cases. We have finally unleashed the entire conformational space of DOPAC; two of the observed conformers, which remained elusive until now, have been irrefutably detected for the first time. This investigation provides relevant insights into the three-dimensional structure of the isolated molecule, probing once more the capability of high-quality rotational data to unveil the shape of relevant organics and biomolecules. Future studies will be focused on the investigation under the isolation conditions granted by the supersonic jet of yet unexplored dopamine metabolites (i.e., adrenaline and noradrenaline), looking forward to tackling the whole metabolic route of dopamine.

CRediT authorship contribution statement

Miguel Sanz-Novo: Writing – original draft, Conceptualization, Formal analysis. **Lucie Kolesniková:** Writing – review & editing, Conceptualization. **Aran Insausti:** Formal analysis, Writing – review & editing. **José L. Alonso:** Writing – review & editing, Conceptualization, Resources, Funding acquisition. **Iker León:** Formal analysis, Writing – review & editing. **Elena R. Alonso:** Supervision, Conceptualization, Methodology, Investigation, Formal analysis, Writing – original draft.

Declaration of Competing Interest

The authors declare that they have no known competing financial interests or personal relationships that could have appeared to influence the work reported in this paper.

Data availability

No data was used for the research described in the article.

Acknowledgments

The authors thank the financial funding from Ministerio de Ciencia e Innovación (CTQ2016-76393-P and PID2019- 111396 GB-I00), Junta de Castilla y León (VA077U16 and VA244P20), and European Research Council under the European Union's Seventh Framework Programme (FP/2007- 2013)/ERC-2013-SyG, Grant Agreement n. 610256 NANOCOSMOS.

Appendix A. Supplementary material

Supplementary data to this article can be found online at https://doi.org/10.1016/j.saa.2022.122303.

References

[1] M. Baldus, GPCR: Lock and key become flexible, Nat. Chem. Biol. 14 (3) (2018) 201–202.
[2] P.A. Insel, et al., GPCRomics: an Approach to Discover GPCR Drug Targets, Trends Pharmacol. Sci. 40 (2019) 378–387.
[3] K. Sriram, P.A. Insel, G protein-coupled receptors as targets for approved drugs: how many targets and how many drugs? Mol. Pharmacol. 93 (2018) 251–258.
[4] E.C. Hirsch, A.M. Graybiel, Y. Agid, Melanized dopaminergic neurons are differentially affected in Parkinson's disease, Nature 334 (1988) 345–348.

[5] B. Bogerts, J. Hantsch, M. Herzer, A morphometric study of the dopamine-containing cell groups in the mesencephalon of normals, Parkinson patients, and schizophrenics, Biol. Psychiatry (1983).
[6] Y. Shao, W. Le, Recent advances and perspectives of metabolomics-based investigations in Parkinson's disease, Mol. Neurodegener. 14 (2019) 1–12.
[7] J. Pu, Y. Liu, S. Gui, L.u. Tian, Y. Yu, X. Song, X. Zhong, X. Chen, W. Chen, P. Zheng, H. Zhang, X. Gong, L. Liu, J. Wu, H. Wang, P. Xie, Metabolomic changes in animal models of depression: a systematic analysis, Mol. Psychiatry 26 (12) (2021) 7328–7336.
[8] P. Uutela, et al., Discovery of dopamine glucuronide in rat and mouse brain microdialysis samples using liquid chromatography tandem mass spectrometry, Anal. Chem. 81 (2009) 427–434.
[9] A. Alaniz-Palacios, A. Martínez-Torres, Antagonistic effect of dopamine structural analogues on human GABAρ1 receptor, Sci. Rep. 7 (2017) 1–11.
[10] H. Deng, H. Hu, Y.e. Fang, Multiple tyrosine metabolites are GPR35 agonists, Sci. Rep. 2 (1) (2012).
[11] W. Zhou, C. Long, A.L. Fink, V.N. Uversky, 3, 4-Dihydroxyphenylacetic Acid (DOPAC) impairs α-synuclein interaction with lipids, Open Proteomics J. 3 (2010) 1–7.
[12] L. Palazzi, B. Fongaro, M. Leri, L. Acquasaliente, M. Stefani, M. Bucciantini, P. Polverino de Laureto, Structural features and toxicity of α-synuclein oligomers grown in the presence of dopac, Int. J. Mol. Sci. 22 (11) (2021) 6008.
[13] W. Zhou, et al., At Low Concentrations, 3,4-Dihydroxyphenylacetic Acid (DOPAC) Binds Non-Covalently to α-Synuclein and Prevents Its Fibrillation, J. Mol. Biol. (2009), https://doi.org/10.1021/nn2045246.Multifunctional.
[14] D.P. Van Kammen, W.B. Van Kammen, L.S. Mann, T. Seppala, M. Linnoila, Dopamine metabolism in the cerebrospinal fluid of drug-free schizophrenic patients with and without cortical atrophy, Arch. Gen. Psychiatry 43 (1986) 978–983.
[15] E. Eldrup, P. Mogensen, J. Jacobsen, H. Pakkenberg, C. Nj, CSF and plasma concentrations of free. 116–121 (1995).
[16] D.S. Goldstein, et al., Biomarkers to detect central dopamine deficiency and distinguish Parkinson disease from multiple system atrophy, Park. Relat. Disord. 14 (2008) 600–607.
[17] D.S. Goldstein, C. Holmes, Y. Sharabi, Cerebrospinal fluid biomarkers of central catecholamine deficiency in Parkinson's disease and other synucleinopathies, Brain 135 (2012) 1900–1913.
[18] H.L. Komiskey, J.F. Bossart, D.D. Miller, P.N. Patil, Conformation of dopamine at the dopamine receptor, Proc. Natl. Acad. Sci. U. S. A. 75 (6) (1978) 2641–2643.
[19] S.K. Callear, A. Johnston, S.E. McLain, S. Imberti, Conformation and interactions of dopamine hydrochloride in solution, J. Chem. Phys. 142 (1) (2015) 014502.
[20] K.H. Wang, A. Penmatsa, E. Gouaux, Neurotransmitter and psychostimulant recognition by the dopamine transporter, Nature 521 (7552) (2015) 322–327.
[21] C. Cabezas, I. Peña, J.C. López, J.L. Alonso, Seven conformers of neutral dopamine revealed in the gas phase, J. Phys. Chem. Lett. 4 (2013) 486–490.
[22] C. Pérez, S. Mata, C. Cabezas, J.C. López, J.L. Alonso, The rotational spectrum of tyrosine, J. Phys. Chem. A 119 (2015) 3731–3735.
[23] M. Sanz-Novo, I. León, E.R. Alonso, J.L. Alonso, Unleashing the shape of l-DOPA at last, Phys. Chem. Chem. Phys. 24 (2022) 3546–3554.
[24] A.J. Lopes Jesus, S. Jarmelo, R. Fausto, I. Reva, Conformational preferences of 3,4-dihydroxyphenylacetic acid (DOPAC). *spectrochim. Acta - Part A Mol*, Biomol. Spectrosc. 140 (2015) 54–64.
[25] N. Okabe, H. Kyoyama, 3,4-Dihydroxyphenylacetic acid. *Acta Crystallogr. Sect. E Struct. Reports*, Online 57 (2001) o715–o716.
[26] J. Meiser, D. Weindl, K. Hiller, Complexity of dopamine metabolism, Cell Commun. Signal. 11 (2013) 1–18.
[27] M.J. Frisch, et al., Gaussian 09 (2009).
[28] E.R. Alonso, I. León, J.L. Alonso, The role of the intramolecular interactions in the structural behavior of biomolecules: Insights from rotational spectroscopy, in: Intra- and Intermolecular Interactions Between Non-covalently Bonded Species, Elsevier, 2021, pp. 93–141.
[29] R.S. Ruoff, T.D. Klots, T. Emilsson, H.S. Gutowsky, Relaxation of conformers and isomers in seeded supersonic jets of inert gases, J. Chem. Phys. 93 (1990) 3142–3150.
[30] P.D. Godfrey, F.M. Rodgers, R.D. Brown, Theory versus experiment in jet spectroscopy: Glycolic acid, J. Am. Chem. Soc. 119 (1997) 2232–2239.
[31] T.F. Miller, D.C. Clary, A.J.H.M. Meijer, Collision-induced conformational changes in glycine, J. Chem. Phys. 122 (24) (2005) 244323.
[32] J.L. Alonso, C. Pérez, M. Eugenia Sanz, J.C. López, S. Blanco, Seven conformers of L-threonine in the gas phase: A LA-MB-FTMW study, Phys. Chem. Chem. Phys. 11 (2009) 617–627.
[33] C. Cabezas, M. Varela, J.L. Alonso, The Structure of the Elusive Simplest Dipeptide Gly-Gly, Angew. Chemie Int. Ed. 56 (2017) 6420–6425.
[34] A.J.L. Jesus, et al., Conformational study of monomeric 2,3-butanediols by matrix-isolation infrared spectroscopy and DFT calculations, J. Phys. Chem. A 110 (2006) 4169–4179.
[35] M.T.S. Rosado, A.J.L. Jesus, I.D. Reva, R. Fausto, J.S. Redinha, Conformational cooling dynamics in matrix-isolated 1,3-butanediol, J. Phys. Chem. A 113 (2009) 7499–7507.